Ore Geology Reviews 72 (2016) 313–322

Contents lists available at ScienceDirect

Ore Geology Reviews

journal homepage: www.elsevier.com/locate/oregeorev

Dating cassiterite using laser ablation ICP-MS

Cong-ying Li [a,*], Rong-qing Zhang [a], Xing Ding [b], Ming-xing Ling [b], Wei-ming Fan [c], Wei-dong Sun [a,c,**]

[a] CAS Key Laboratory of Mineralogy and Metallogeny, Guangzhou Institute of Geochemistry, Chinese Academy of Sciences, Guangzhou 510640, China
[b] State Key Laboratory of Isotope Geochemistry, Guangzhou Institute of Geochemistry, Chinese Academy of Sciences, Guangzhou 510640, China
[c] CAS Center for Excellence in Tibetan Plateau Earth Sciences, Chinese Academy of Sciences, Beijing 100101, China

ARTICLE INFO

Article history:
Received 13 March 2015
Received in revised form 17 July 2015
Accepted 21 July 2015
Available online 23 July 2015

Keywords:
Cassiterite
U–Pb dating
Laser ablation ICP-MS
Tera–Wasserburg U–Pb intercept age
LA-ICP-MS

ABSTRACT

Cassiterite is the main ore mineral of Sn deposits, and may be used to date tin mineralization processes/processes. Both isotope dilution thermal ionization mass spectrometer (ID-TIMS) and laser ablation multi-collector inductively coupled plasma mass spectrometer (LA-MC-ICP-MS) have been applied to cassiterite U–Pb dating. Here we show that cassiterite U–Pb dating results using LA-ICP-MS are comparable to those using LA-MC-ICP-MS. Our results also show that Tera–Wasserburg U–Pb intercept age is far better than the previously used $^{206}Pb/^{207}Pb$ versus $^{238}U/^{207}Pb$ "isochron" age because the latter weighted data points with low proportions of common Pb more heavily, such that introducing larger errors. Moreover, $^{206}Pb_i/^{207}Pb$ changes with age and $^{238}U/^{207}Pb$ ratios, such that yields results younger than the real ages with larger errors. Samples with multiple common Pb sources are difficult to date. Nevertheless, multiple common Pb in cassiterite are often associated with fluid inclusions that may be identified and avoided. The precisions of cassiterite U–Pb ages are not as good as zircon ages, but they provide direct dating on the mineralization processes/processes. Therefore, coupled studies on zircon and cassiterite dating may provide constraints on the relation between magmatism ± hydrothermal activities and mineralization.

© 2015 Elsevier B.V. All rights reserved.

1. Introduction

Cassiterite (SnO_2) is the main ore mineral of Sn deposits. It belongs to the rutile group ($M^{4+}O_2$), which in principle should have high U and low common Pb contents in its lattice. Cassiterite U–Pb ages directly date tin mineralization processes/processes (Gulson and Jones, 1993; Liu et al., 2007b; Yuan et al., 2008). This is an advantage over U–Pb dating on zircon and rutile (Gulson and Jones, 1992), and $^{40}Ar/^{39}Ar$ dating on muscovite and even fluid inclusions in cassiterite and wolframite (Bai et al., 2013), which date magmatism and fluid activities, respectively, such that it may not necessarily represent the mineralization age.

Cassiterite, however, usually has common Pb contents much higher than those of zircon. Moreover, the U content of cassiterite is generally at low ppm levels, which is much lower than that of zircon, and even rutile and titanite, etc., with higher common Pb proportions. As a result, published ID-TIMS cassiterite U–Pb ages have errors considerably larger than those of LA-ICP-MS U–Pb ages of zircon and many other high-U minerals. In particular, cassiterite formed during hydrothermal processes may contain mineral/fluid inclusions with non-equilibrium common Pb that is harmful to high quality isotope dating (Clayton and Rojkovic, 1999).

In recent years, in situ laser ablation-multicollector-inductively coupled plasma-mass spectrometry (LA-MC-ICP-MS) U–Pb dating on cassiterite yields $^{206}Pb/^{207}Pb$ versus $^{238}U/^{207}Pb$ "isochron" ages (Chen et al., 2014; Ma et al., 2013; Wang et al., 2014; Xie et al., 2013; Yuan et al., 2011; Zhang et al., 2013, 2014) seemingly comparable to ID-TIMS results. Nevertheless, some of the samples cannot yield reasonable isochron ages, which makes this method unpopular.

Here we try to evaluate and optimize in situ cassiterite U–Pb dating method using LA-ICP-MS. Our results show that Tera–Wasserburg U–Pb lower intercept age is better than $^{206}Pb/^{207}Pb$ versus $^{238}U/^{207}Pb$ "isochron" age, because the former is controlled mainly by $^{238}U/^{206}Pb$ ratios of data points with lower proportions of common Pb and thus higher $^{206}Pb/^{207}Pb$ and $^{238}U/^{207}Pb$ values. It is also suggested that cassiterite U–Pb dating results using LA-ICP-MS (with quadrupole mass spectrometer) are comparable to those of LA-MC-ICP-MS.

2. Sample preparation and analytical methods

2.1. Sample preparation

Cassiterite samples from Hehuaping Sn–Pb–Zn deposit of the Nanling Range, South China and Xuebaoding Sn–W–Be deposit in the Songpan–Garzê orogenic belt southwest China have been analyzed in

* Corresponding author.
** Correspondence to: W.-D. Sun, CAS Key Laboratory of Mineralogy and Metallogeny, Guangzhou Institute of Geochemistry, Chinese Academy of Sciences, Guangzhou 510640, China.
E-mail addresses: licongying18@163.com (C. Li), weidongsun@gig.ac.cn (W. Sun).

http://dx.doi.org/10.1016/j.oregeorev.2015.07.016
0169-1368/© 2015 Elsevier B.V. All rights reserved.

this contribution. Both deposits have been previously dated using other methods (Liu et al., 2007a, 2010; Zhang et al., 2014, 2015).

The Hehuaping tin polymetallic deposit is located to the southeast of the Wangxianling pluton in the Middle Nanling Range, near Chenzhou City, South China. Tin mineralization is spatially associated with a Late Jurassic (~156 Ma) hidden biotite granite pluton and granite porphyry dykes, both of which have affinities of A_2-type granite (Zhang et al., 2015). The proximal skarn cassiterite–magnetite orebody is 3400 m long, 300–600 m wide and 5.01–16.09 m thick, and is strata-bound and sheet-like at the bottom of the skarn, with a proven reserve of 27.4 Mt at 0.72% Sn and coexisting Pb, Zn (0.162 Mt Pb + Zn ore at 2.9% Pb and 3.5% Zn), and minor Mn and Bi. A well-defined mineralization zonation is observed from a fresh coarse-grained biotite granite towards the limestone. The alteration zoning begins with greisenized granite, through quartz-rich greisen, quartz–fluorite vein bearing sericitized sandstone, cassiterite–magnetite skarn, forsterite–spinel–diopside skarn, serpentine–talc–phlogopite skarn, to cassiterite–sulfide bearing marble (Yao et al., 2014). Greisen orebodies are NE-trending and are developed mainly in the roof part of biotite granite dykes in the east. Cassiterite in the greisen is brownish black and coexists with quartz and muscovite. Those coexisting with magnetite are very small (<100 μm) and usually reddish brown. The U–Pb "isochron" ages of cassiterite grains from greisen and skarn ores of the Hehuaping deposit are 154.8 ± 5.8 Ma and 157.8 ± 4.1 Ma, showing that the Sn mineralization occurred at a similar time to the Late Jurassic granitic magmatism (Zhang et al., 2015). Two types of cassiterite were studied here. Sample IV was obtained from the skarn orebody in the southwest of the mining district, and sample WXL-17 was collected from the greisen ore in the east.

The Xuebaoding Sn–Be deposit is located to the north of Longmenshan, near Pingwu county, southwest China. The potential reserves of Sn and W metal of this deposit are 49,000 t and 271 t, respectively. Detailed description of geological characteristics, and study on mineralogy and chronology of this deposit has been reported by previous authors (Liu et al., 2007a, 2010, 2012a,b). This deposit is well known for producing coarse-grained crystals of scheelite, beryl, cassiterite, fluorite and other minerals (Liu et al., 2012a,b). Spatially and temporally, it is related to the Pukouling and Pankou muscovite granites with muscovite $^{40}Ar/^{39}Ar$ plateau ages of 200 Ma and 193 Ma, respectively (Liu et al., 2010). The Xuebaoding deposit consists of about 40 ore veins, striking nearly N and dipping 10° to 55°E. The veins are commonly 100 m long and 0.3–3 m thick, with interval from 1 to 10 m between two neighboring veins (Liu et al., 2012a,b). The ore veins extend from the roof of granitic intrusion to the marble. Cassiterite and scheelite mainly occur in the veins cutting marble. The Sm–Nd dating on scheelite of the ore vein gave an age of 182.0 ± 9.2 Ma (Liu et al., 2007a). The $^{40}Ar/^{39}Ar$ isochron age (194.5 ± 1.0 Ma) of muscovite is consistent with a U–Pb age (193.6 ± 6 Ma) of the coexisting cassiterite from the ore vein, both of which approximate the emplacement age of the granitic intrusion in the Xuebaoding deposit (Zhang et al., 2014). Black cassiterite crystal (XBD) in this study was collected from a cassiterite–muscovite vein.

2.2. Analytical methods

Ore samples (WXL17 and IV) were crushed to 40–60 mesh, and cassiterite grains were separated using conventional magnetic and heavy liquid separation techniques. Cassiterite grains were then handpicked under a binocular microscope. A large cassiterite crystal of ~2 cm in diameter from sample XBD was cut into two pieces. Cassiterite grains were mounted in epoxy, and then polished down to near half sections to expose internal structures.

Cassiterite samples are checked carefully under the microscope, electron microprobe (EMP) and scanning electron microscope (SEM) to observe mineral and fluid inclusions and cracks. Most cassiterite grains from the Hehuaping deposit have abundant fluid inclusions (Fig. 1A and B) and mineral inclusions, such as galena, pyrite and quartz (Fig. 1C and D), with some cracks but no clear growth oscillatory zones. The large cassiterite crystal from the Xuebaoding deposit has relatively homogeneous composition and mineral inclusions are rare (Fig. 1E).

U–Pb dating was carried out using a LA-ICP-MS system in the CAS Key Laboratory of Mineralogy and Metallogeny, Guangzhou Institute of Geochemistry, the Chinese Academy of Sciences. The system consists of an Agilent 7900 ICP-MS coupled with a Resonetics RESOlution S-155 laser. This laser ablation system is equipped with a large sample cell (155 mm × 105 mm), which can host 20 epoxy sample mounts (with diameter of 25.4 mm). It can wash out 99% signal within less than 1.5 s, because of its two-volume laser-ablation cell. A Squid smoothing device was used to reduce statistic error induced by laser-ablation pulses and improve the quality of data (Li et al., 2012; Tu et al., 2011). Helium gas carrying the ablated sample aerosol is mixed with argon carrier gas and nitrogen as additional di-atomic gas to enhance sensitivity, and finally flows into ICP. Prior to analysis, the LA-ICP-MS system was optimized using NIST610 ablated with 29 μm spot size and 5 μm/s scan speed to achieve maximum signal intensity and low oxide rates. The spot size is adjustable (4–200 μm) and laser pulse frequency ranges from 1 to 20 Hz. Samples from Hehuaping were analyzed using different laser energy densities from 1.8 J/cm^2, 4 J/cm^2 and 8 J/cm^2, a spot size of 74 μm and repetition rates of 6 Hz and 12 Hz. Other samples were analyzed using an energy density of 4 J/cm^2, a spot size of 74 μm and a repetition rate of 6 Hz. NIST SRM 610 and an in-lab cassiterite standard AY-4 were used as an external calibration standard. AY-4 was collected from the No. 19 skarn orebody in the Anyuan tin deposit of the Furong orefield in the middle Nanling Range. This cassiterite sample has been well studied using ID-TIMS with a U–Pb age of 158.2 ± 0.4 Ma (Yuan et al., 2011). It also has very low common lead. NIST SRM 610 was analyzed twice for every ten analyses; AY-4 was analyzed twice for every five analyses. Each spot analysis incorporated a background acquisition of approximately 20 s followed by 40 s sample data acquisition. Isotopes were measured in time-resolved mode. For U/Pb dating, dwell times for each mass scan are 15 ms for ^{204}Pb, ^{206}Pb, ^{208}Pb, ^{238}U, and ^{235}U and 25 ms for ^{207}Pb. The detailed instrumentation and operating conditions

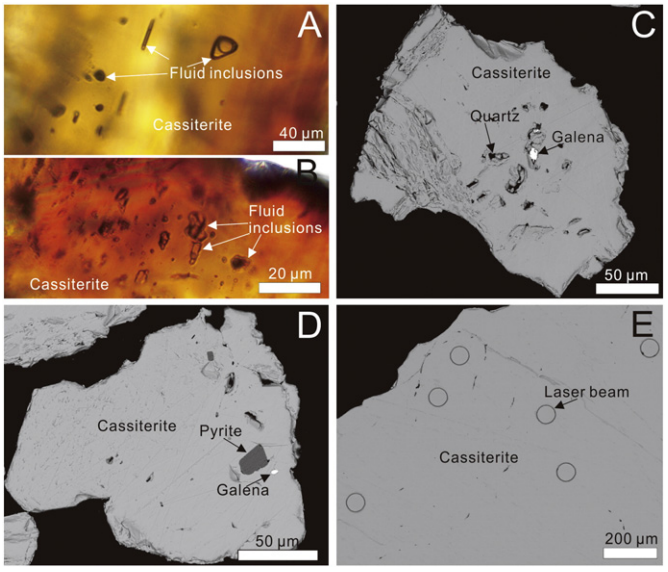

Fig. 1. Photomicrographs and BSE images of cassiterite grains and crystal piece. (A) Photomicrograph of two phase fluid inclusions in cassiterite grains from tin greisen in the Hehuaping deposit (plane light). (B) Photomicrograph of abundant two phase fluid inclusions in cassiterite grains from tin skarn in the Hehuaping deposit (plane light). (C) BSE image showing that galena and quartz are enclosed in cassiterite grains from tin greisen in the Hehuaping deposit. (D) BSE image showing that galena and pyrite are enclosed in cassiterite grains from tin skarn in the Hehuaping deposit. (E). BSE image of cassiterite showing relatively homogeneous composition and lacking of mineral inclusions from cassiterite–muscovite vein in the Xuebaoding deposit.

Table 1
LA-ICP-MS instrumentation and operating conditions.

Resolution S-155 laser ablation system (ArF Excimer, Resonetics LLC, USA)	
Laser wavelength	193 nm
Pulse width	~20 ns
Fluence	4 J/cm^2, 8 J/cm^2 and 12 J/cm^2
Repetition rate	6 Hz and 12 Hz
Spot size	74 μm
Carrier gas	0.35 l/min He
Ablation duration	40 s
Angilent 7900x ICP-MS	
Sample introduction	Ablation aerosol
Forward power	1250 w
Ar cooling gas flow rate	15 l/min
Ar auxiliary gas flow rate	0.75 l/min
Ni sampling cone orifice	1.0 mm
Ni skimmer cone orifice	0.7 mm
Acquisition mode	Peak jumping
Channel dwell time	20 ms
Channel per mass	1
Measured isotopes	^{204}Pb, ^{206}Pb, ^{207}Pb, ^{208}Pb, ^{232}Th and ^{238}U
Other information	
Gas blank	30 s on-peak zero subtracted
Washing time	30 s after the laser ended firing

are given in Table 1. Isoplot 3.23 (Ludwing, 2003) was used to calculate the U–Pb age. Data errors of single spot are 1σ and those of weighted average ^{206}Pb/^{238}U ages are 2σ.

3. Results

In order to achieve the best working conditions, cassiterite samples from the Hehuaping deposit were analyzed three times, using different laser energy densities and repetition rates. The dating results are listed in Tables 2–5. Concordia, Tera–Wasserburg lower intercept ages and ^{206}Pb/^{207}Pb versus ^{238}U/^{207}Pb "isochron" diagrams for results under different conditions are shown in Figs. 2–5.

Sixty single spot U/Pb analyses were measured by LA-ICP-MS with a laser beam diameter of 74 μm, a beam energy density of 4 J/cm^2 and a repetition rate of 6 Hz. Fifteen out of the 60 analyses were excluded based on two criteria for good analyses. First, no obvious inclusions were ablated during the analyses; second, the dwell time for the analyses was longer than 30 s. The remaining analyses yielded a U–Pb concordia lower intercept age of 158.4 ± 4.3 Ma (MSWD = 8.4), U–Pb Tera–Wasserburg concordia lower intercept age of 158.9 ± 4.5 Ma (MSWD = 9.0) and a ^{206}Pb/^{207}Pb–^{238}U/^{207}Pb isochron age of 149.9 ± 9.5 Ma with initial ^{206}Pb/^{207}Pb ratio of 1.575 ± 0.087 (with errors at a

Table 2
U–Pb isotopic data of cassiterite from the Hehuaping deposit (Group one).

	U (ppm)	Th (ppm)	^{207}Pb/^{206}Pb	1σ	^{207}Pb/^{235}U	1σ	^{206}Pb/^{238}U	1σ	^{238}U/^{207}Pb	Err (%)	^{206}Pb/^{207}Pb	Err (%)
WXL-17-01	2.3	0.0	0.13631	0.01564	0.60219	0.06419	0.03260	0.00162	225.07	10.66	7.34	11.47
WXL-17-03	6.1	1.1	0.30230	0.01820	1.72982	0.11303	0.04119	0.00146	80.30	6.53	3.31	6.02
WXL-17-04	4.3	0.0	0.10962	0.01282	0.42172	0.04361	0.02880	0.00105	316.71	10.34	9.12	11.69
WXL-17-05	1.6	0.0	0.67989	0.02839	45.30303	2.34852	0.48073	0.01678	3.06	5.18	1.47	4.18
WXL-17-06	7.6	0.0	0.04927	0.00951	0.16535	0.02769	0.02531	0.00107	801.85	16.75	20.30	19.30
WXL-17-07	1.1	0.0	0.13368	0.02875	0.35027	0.05301	0.02374	0.00191	315.17	15.13	7.48	21.50
WXL-17-09	4.1	1.0	0.22248	0.02548	1.35300	0.21903	0.04078	0.00274	110.21	16.19	4.50	11.45
WXL-17-10	3.1	0.2	0.46939	0.02292	8.64712	0.53574	0.13268	0.00610	16.06	6.20	2.13	4.88
WXL-17-11	4.7	0.1	0.38417	0.02055	3.63605	0.18506	0.06846	0.00191	38.02	5.09	2.60	5.35
WXL-17-12	4.8	0.2	0.30486	0.01945	2.15859	0.18357	0.05032	0.00179	65.19	8.50	3.28	6.38
WXL-17-20	2.3	0.0	0.15001	0.02104	0.62138	0.09405	0.03022	0.00186	220.61	15.14	6.67	14.03
WXL17-201	3.5	0.2	0.31809	0.03917	1.35180	0.14407	0.03082	0.00198	102.00	10.66	3.14	12.31
WXL17-203	3.5	0.2	0.41554	0.01662	6.16403	0.64512	0.10410	0.00868	23.12	10.47	2.41	4.00
WXL17-204	5.1	0.1	0.35712	0.01514	4.43365	0.25539	0.09091	0.00483	30.80	5.76	2.80	4.24
WXL17-205	4.2	0.2	0.24844	0.01209	1.67143	0.08817	0.04890	0.00139	82.31	5.28	4.03	4.87
WXL17-207	1.9	0.0	0.10947	0.01265	0.41214	0.03901	0.02908	0.00106	314.11	9.47	9.14	11.56
WXL17-208	4.9	0.0	0.06891	0.00589	0.23548	0.02014	0.02485	0.00049	583.91	8.55	14.51	8.55
WXL17-209	6.5	0.4	0.35973	0.01545	3.58258	0.27373	0.07074	0.00366	39.30	7.64	2.78	4.30
WXL17-210	4.0	0.1	0.34457	0.01726	2.73304	0.17498	0.05657	0.00207	51.30	6.40	2.90	5.01
WXL17-211	4.0	0.1	0.28674	0.01441	1.59916	0.07700	0.04109	0.00104	84.88	4.82	3.49	5.03
WXL17-213	3.5	0.0	0.25124	0.02335	1.11953	0.08352	0.03347	0.00087	118.93	7.46	3.98	9.29
WXL17-214	7.5	0.0	0.56467	0.01951	16.72159	1.73048	0.20419	0.01757	8.67	10.35	1.77	3.46
WXL17-215	4.7	0.1	0.60891	0.02287	16.93508	0.90860	0.20110	0.00667	8.17	5.37	1.64	3.76
WXL17-216	3.1	0.1	0.64424	0.02773	47.78603	6.35461	0.50880	0.05820	3.05	13.30	1.55	4.30
WXL17-217	3.0	0.0	0.08520	0.00878	0.30374	0.03373	0.02608	0.00067	449.95	11.11	11.74	10.31
WXL17-218	3.1	0.1	0.54323	0.02064	6.00800	0.20405	0.08115	0.00150	22.68	3.40	1.84	3.80
WXL17-219	7.7	0.0	0.13096	0.00791	0.51327	0.03517	0.02807	0.00060	272.09	6.85	7.64	6.04
WXL17-221	11.1	0.0	0.23403	0.01546	1.32408	0.11908	0.03781	0.00135	113.02	8.99	4.27	6.61
WXL17-222	1.7	0.0	0.22546	0.02221	1.35044	0.17872	0.04058	0.00236	109.31	13.23	4.44	9.85
WXL17-224	11.6	0.0	0.03555	0.00273	0.11358	0.00854	0.02364	0.00040	1189.89	7.52	28.13	7.67
WXL17-225	3.3	0.0	0.13537	0.01043	0.50315	0.03660	0.02822	0.00076	261.81	7.27	7.39	7.71
WXL17-226	10.5	0.2	0.46308	0.01387	7.74787	0.50314	0.11921	0.00566	18.11	6.49	2.16	2.99
WXL17-227	2.2	0.0	0.07754	0.01042	0.26892	0.03145	0.02666	0.00098	483.73	11.70	12.90	13.44
WXL17-228	4.3	0.1	0.47147	0.03509	4.98243	0.52293	0.07322	0.00523	28.97	10.50	2.12	7.44
WXL17-229	4.7	0.0	0.04925	0.00559	0.17432	0.01969	0.02566	0.00074	791.40	11.30	20.30	11.34
WXL17-231	12.6	0.0	0.08433	0.00593	0.30436	0.02070	0.02622	0.00041	452.22	6.80	11.86	7.03
WXL17-232	2.7	0.0	0.32147	0.02317	2.06510	0.24088	0.04185	0.00235	74.33	11.66	3.11	7.21
WXL17-233	14.7	0.0	0.08989	0.00726	0.34745	0.03241	0.02723	0.00049	408.50	9.33	11.13	8.08
WXL17-234	4.3	0.0	0.04685	0.00558	0.16629	0.01932	0.02562	0.00064	833.16	11.62	21.35	11.92
WXL17-235	1.9	0.0	0.08383	0.01348	0.29005	0.04139	0.02742	0.00140	435.09	14.27	11.93	16.08
WXL17-236	12.7	0.1	0.55154	0.02080	6.75165	0.26728	0.08856	0.00115	20.47	3.96	1.81	3.77
WXL17-237	2.6	0.0	0.38718	0.02351	2.78343	0.21839	0.05166	0.00248	49.99	7.85	2.58	6.07
WXL17-239	12.4	0.1	0.30300	0.01950	2.29508	0.33056	0.04675	0.00351	70.60	14.40	3.30	6.44
WXL17-240	5.2	0.0	0.03877	0.00441	0.13535	0.01439	0.02539	0.00052	1015.88	10.63	25.79	11.37
WXL17-241	4.2	0.0	0.03999	0.00502	0.13276	0.01647	0.02401	0.00074	1041.73	12.41	25.01	12.55

Table 3
U–Pb isotopic data of cassiterite from the Hehuaping deposit (Group two).

	U (ppm)	Th (ppm)	$^{207}Pb/^{206}Pb$	1σ	$^{207}Pb/^{235}U$	1σ	$^{206}Pb/^{238}U$	1σ	$^{238}U/^{207}Pb$	Err (%)	$^{206}Pb/^{207}Pb$	Err (%)
WXL17-244	1.0	0.0	0.22930	0.01710	1.59142	0.18133	0.03789	0.00298	115.10	11.39	4.36	7.46
WXL17-246	5.3	0.0	0.54741	0.01236	18.15080	0.66946	0.24172	0.00773	7.56	3.69	1.83	2.26
WXL17-248	5.9	0.0	0.25341	0.00693	1.39684	0.04734	0.04026	0.00079	98.01	3.39	3.95	2.73
WXL17-249	7.8	0.3	0.34632	0.01085	3.06007	0.17505	0.06317	0.00224	45.71	5.72	2.89	3.13
WXL17-250	5.1	0.0	0.09838	0.00659	0.37677	0.02752	0.02794	0.00046	363.81	7.31	10.16	6.70
WXL17-251	3.4	0.0	0.18165	0.01602	0.58493	0.05285	0.02696	0.00230	204.15	9.04	5.51	8.82
WXL17-252	2.8	0.0	0.15880	0.01159	0.42991	0.02818	0.02378	0.00207	264.84	6.56	6.30	7.30
WXL17-253	4.2	0.0	0.06232	0.00523	0.10553	0.00872	0.01617	0.00174	992.29	8.26	16.05	8.39
WXL17-254	8.0	0.0	0.12241	0.01043	0.21854	0.02201	0.01954	0.00260	418.06	10.07	8.17	8.52
WXL17-256	3.6	0.1	0.35471	0.02524	6.47552	0.93058	0.15969	0.02908	17.66	14.37	2.82	7.12
WXL17-257	2.0	0.0	0.15378	0.01536	0.54489	0.07471	0.02310	0.00253	281.51	13.71	6.50	9.99
WXL17-259	6.7	0.0	0.21782	0.01452	0.99568	0.09251	0.02968	0.00142	154.68	9.29	4.59	6.67
WXL17-260	2.3	0.0	0.30787	0.01588	1.56919	0.09618	0.03591	0.00122	90.45	6.13	3.25	5.16
WXL17-261	4.9	0.0	0.07328	0.00590	0.24845	0.01690	0.02531	0.00051	539.10	6.80	13.65	8.05
WXL17-262	0.9	0.0	0.04377	0.00791	0.14281	0.02605	0.02519	0.00110	906.83	18.24	22.85	18.07
WXL17-263	7.7	0.1	0.45480	0.03152	11.53970	2.18502	0.14251	0.02240	15.43	18.94	2.20	6.93
WXL17-264	5.5	0.2	0.60722	0.01280	21.38030	0.52537	0.25481	0.00355	6.46	2.46	1.65	2.11
WXL17-265	5.7	0.0	0.11687	0.00600	0.44090	0.02245	0.02756	0.00052	310.42	5.09	8.56	5.14
WXL17-267	4.1	0.0	0.08340	0.00657	0.28554	0.02126	0.02597	0.00061	461.63	7.45	11.99	7.87
WXL17-268	3.1	0.0	0.46439	0.01427	17.04530	0.66914	0.27532	0.00587	7.82	3.93	2.15	3.07
WXL17-269	4.3	0.3	0.33290	0.01404	3.25482	0.18513	0.07415	0.00209	40.51	5.69	3.00	4.22
WXL17-270	1.6	0.0	0.04775	0.00716	0.13544	0.01917	0.02359	0.00079	887.64	14.15	20.94	15.00
WXL17-272	2.9	0.0	0.05507	0.00448	0.13192	0.01367	0.02123	0.00106	855.30	10.37	18.16	8.14
WXL17-274	2.8	0.1	0.17828	0.00868	1.46956	0.19668	0.07602	0.00744	73.78	13.38	5.61	4.87
WXL17-275	6.1	0.1	0.05938	0.00378	0.10366	0.01387	0.01903	0.00144	885.09	13.38	16.84	6.36
WXL17-276	4.5	0.3	0.16693	0.00719	0.90837	0.08184	0.04868	0.00334	123.06	9.01	5.99	4.31
WXL17-277	4.6	0.0	0.21751	0.01244	12.75730	1.98620	0.37206	0.05544	12.36	15.57	4.60	5.72
WXL17-279	10.8	0.4	0.26605	0.00835	2.61974	0.13150	0.07103	0.00237	52.92	5.02	3.76	3.14
WXL17-280	8.0	0.4	0.33145	0.01099	5.09620	0.30107	0.11058	0.00432	27.28	5.91	3.02	3.32

95% confidence level, MSWD = 2.0) (Fig. 2). The isochron age is much younger than both the lower intercept ages.

In the second group, 40 spots were analyzed using a laser beam diameter of 74 μm, with an energy density of 8 J/cm^2 and a repetition rate of 6 Hz. From this data set, 10 analyses were excluded based on the same criteria mentioned above. The remaining analyses, however, still show two different trends, indicating different sources of common Pb. This is likely because of more common Pb from fluid and/or mineral inclusions due to high energy and consequently faster ablations. For analyses with less common Pb (symbols with solid lines), the U–Pb concordia lower intercept age is 156.0 ± 6.8 Ma (MSWD = 9.2); the U–Pb Tera–Wasserburg concordia lower intercept age is 157.2 ±

Table 4
U–Pb isotopic data of cassiterite from the Hehuaping deposit (Group three).

	U (ppm)	Th (ppm)	$^{207}Pb/^{206}Pb$	1σ	$^{207}Pb/^{235}U$	1σ	$^{206}Pb/^{238}U$	1σ	$^{238}U/^{207}Pb$	Err (%)	$^{206}Pb/^{207}Pb$	Err (%)
WXL17-301	7.2	0.0	0.40398	0.01772	3.82600	0.21260	0.06802	0.00194	36.39	5.56	2.48	4.39
WXL17-302	6.5	1.4	0.40497	0.01612	4.82619	0.25154	0.08576	0.00252	28.80	5.21	2.47	3.98
WXL17-303	5.0	2.4	0.41582	0.01693	4.73741	0.22180	0.08333	0.00231	28.86	4.68	2.41	4.07
WXL17-304	2.2	0.0	0.06495	0.01237	0.23408	0.06543	0.02510	0.00118	613.38	27.95	15.40	19.04
WXL17-305	3.3	0.1	0.26147	0.01607	1.60820	0.10218	0.04592	0.00128	83.29	6.35	3.83	6.15
WXL17-307	2.4	0.0	0.10451	0.01092	0.43712	0.05062	0.02930	0.00154	326.61	11.58	9.57	10.45
WXL17-309	2.6	0.0	0.05356	0.00742	0.20197	0.02605	0.02727	0.00108	684.52	12.90	18.67	13.85
WXL17-310	3.9	0.1	0.20895	0.01363	0.96484	0.05870	0.03355	0.00112	142.67	6.08	4.79	6.52
WXL17-311	8.0	0.0	0.08555	0.00633	0.31300	0.02194	0.02643	0.00074	442.24	7.01	11.69	7.39
WXL17-312	5.4	0.0	0.23344	0.01335	1.16730	0.05449	0.03703	0.00131	115.69	4.67	4.28	5.72
WXL17-313	4.5	0.0	0.13583	0.00906	0.54944	0.03567	0.02905	0.00092	253.46	6.49	7.36	6.67
WXL17-314	8.8	0.0	0.28901	0.02553	2.73443	0.47483	0.05261	0.00521	65.77	17.37	3.46	8.83
WXL17-315	3.3	0.0	0.19437	0.01349	0.83391	0.05883	0.03173	0.00135	162.15	7.06	5.15	6.94
WXL17-316	7.3	0.3	0.47360	0.01668	4.86838	0.15784	0.07455	0.00164	28.32	3.24	2.11	3.52
WXL17-317	8.6	1.3	0.41402	0.01409	3.65945	0.15350	0.06351	0.00163	38.03	4.20	2.42	3.40
WXL17-318	8.2	0.8	0.18331	0.01344	0.91534	0.11067	0.03323	0.00141	164.14	12.09	5.46	7.33
WXL17-319	2.3	0.0	0.07397	0.01030	0.27917	0.03757	0.02723	0.00106	496.47	13.46	13.52	13.93
WXL17-320	1.4	0.0	0.43118	0.03067	2.67898	0.19630	0.04838	0.00316	47.94	7.33	2.32	7.11
WXL17-321	0.8	0.0	0.10427	0.02501	0.27590	0.03741	0.02825	0.00233	339.42	13.56	9.59	23.99
WXL17-322	4.8	0.0	0.04135	0.00570	0.15149	0.01719	0.02820	0.00095	857.37	11.34	24.18	13.79
WXL17-323	6.4	0.0	0.17973	0.01878	1.04188	0.19047	0.03453	0.00221	161.14	18.28	5.56	10.45
WXL17-324	4.6	0.0	0.27163	0.01755	1.68240	0.15660	0.04197	0.00187	87.73	9.31	3.68	6.46
WXL17-325	2.9	0.0	0.41404	0.02543	4.31723	0.33684	0.07443	0.00432	32.45	7.80	2.42	6.14
WXL17-326	3.7	0.0	0.19577	0.01814	0.99103	0.14900	0.03409	0.00171	149.82	15.04	5.11	9.27
WXL17-327	0.6	0.0	0.10803	0.02611	0.24389	0.03441	0.02325	0.00208	398.10	14.11	9.26	24.17
WXL17-328	5.5	0.0	0.17243	0.01631	0.67236	0.07158	0.02701	0.00089	214.74	10.65	5.80	9.46
WXL17-329	11.7	1.0	0.16727	0.00859	0.67792	0.03065	0.02945	0.00073	202.97	4.52	5.98	5.14
WXL17-330	5.8	0.1	0.44223	0.02474	3.13958	0.26659	0.04906	0.00250	46.09	8.49	2.26	5.59

Table 5
U–Pb isotopic data of cassiterite from the Hehuaping deposit (Tin skarn).

	U (ppm)	Th (ppm)	$^{207}Pb/^{206}Pb$	1σ	$^{207}Pb/^{235}U$	1σ	$^{206}Pb/^{238}U$	1σ	$^{238}U/^{207}Pb$	Err (%)	$^{206}Pb/^{207}Pb$	Err (%)
IV-1-01	4.1	0.0	0.08898	0.01480	0.29584	0.04543	0.02340	0.00112	480.25	15.36	11.24	16.64
IV-1-02	3.0	0.0	0.05740	0.01546	0.18209	0.04382	0.02617	0.00116	665.73	24.07	17.42	26.93
IV-1-03	1.6	0.0	0.39380	0.05544	2.70647	0.30477	0.05694	0.00441	44.60	11.26	2.54	14.08
IV-1-05	6.4	0.0	0.05368	0.00877	0.17329	0.02362	0.02452	0.00091	759.73	13.63	18.63	16.33
IV-1-06	2.0	0.0	0.14525	0.03381	0.36196	0.07432	0.02393	0.00232	287.70	20.53	6.89	23.28
IV-1-07	10.3	0.0	0.02080	0.00330	0.05427	0.00979	0.01989	0.00121	2417.82	18.03	48.09	15.86
IV-1-08	2.1	0.0	0.03140	0.00577	0.08065	0.01382	0.02253	0.00173	1413.20	17.14	31.84	18.37
IV-1-09	6.1	0.0	0.05724	0.01377	0.17033	0.05875	0.02183	0.00190	800.28	34.49	17.47	24.05
IV-1-10	18.5	0.0	0.08618	0.01451	0.28955	0.09348	0.02661	0.00335	436.11	32.29	11.60	16.83
IV-1-11	1.1	0.0	0.25607	0.03982	2.63639	0.70583	0.06030	0.01024	64.77	26.77	3.91	15.55
IV-1-12	11.7	0.0	0.02974	0.00450	0.09446	0.01404	0.02280	0.00087	1474.65	14.86	33.62	15.12
IV-1-13	4.4	0.0	0.41833	0.03379	10.35999	1.32453	0.17795	0.01800	13.43	12.79	2.39	8.08
IV-1-14	1.0	0.0	0.45766	0.05637	9.04104	2.09404	0.14600	0.02604	14.97	23.16	2.19	12.32
IV-1-15	9.1	0.0	0.02756	0.00567	0.09201	0.01920	0.02450	0.00098	1481.00	20.86	36.28	20.56
IV-1-16	5.3	0.0	0.06403	0.01161	0.18117	0.02529	0.02281	0.00101	684.68	13.96	15.62	18.14
IV-1-17	4.1	0.0	0.21834	0.03514	1.84829	0.60184	0.04764	0.00752	96.13	32.56	4.58	16.09
IV-1-18	6.8	0.0	0.25358	0.03610	2.33240	0.55444	0.05122	0.00649	76.99	23.77	3.94	14.24
IV-1-19	2.2	0.0	0.31231	0.05224	7.94330	2.64499	0.11633	0.02874	27.53	33.30	3.20	16.73
IV-1-20	2.8	0.0	0.23574	0.02913	3.19419	0.83722	0.11997	0.04524	35.36	26.21	4.24	12.36
IV-2-01	6.3	0.0	0.41412	0.04793	15.56413	3.41496	0.29235	0.04393	8.26	21.94	2.42	11.57
IV-2-02	4.2	0.0	0.39275	0.04111	8.15056	1.34444	0.16703	0.01082	15.24	16.50	2.55	10.47
IV-2-04	3.4	0.0	0.32136	0.04549	4.02476	1.03506	0.09279	0.01156	33.53	25.72	3.11	14.16
IV-2-05	5.2	0.0	0.37810	0.05017	14.20739	4.85052	0.28316	0.06512	9.34	34.14	2.65	13.27
IV-2-06	6.0	0.0	0.29183	0.04106	2.97570	0.76921	0.06306	0.00995	54.34	25.85	3.43	14.07
IV-2-08	5.1	0.0	0.69057	0.04634	31.55115	3.64672	0.33743	0.02911	4.29	11.56	1.45	6.71
IV-2-11	3.3	0.0	0.38342	0.02903	3.49068	0.39046	0.06499	0.00494	40.13	11.19	2.61	7.57
IV-2-15	9.8	0.0	0.13062	0.00958	0.55020	0.04296	0.03027	0.00074	252.89	7.81	7.66	7.34
IV-2-16	5.5	0.0	0.31652	0.02647	2.88079	0.37619	0.06750	0.00612	46.81	13.06	3.16	8.36
IV-2-17	4.0	0.0	0.40750	0.03381	13.13423	2.11836	0.26097	0.03764	9.40	16.13	2.45	8.30
IV-2-18	1.9	0.0	0.32899	0.03471	10.32655	2.75744	0.24586	0.05441	12.36	26.70	3.04	10.55
IV-2-19	5.0	0.0	0.28910	0.03430	6.48129	1.69014	0.19466	0.04098	17.77	26.08	3.46	11.87
IV-2-20	35.3	0.1	0.27567	0.03744	3.46571	0.86454	0.13421	0.01582	27.03	24.95	3.63	13.58

6.2 Ma (MSWD = 7.4). Remarkably, the $^{206}Pb/^{207}Pb$–$^{238}U/^{207}Pb$ isochron age is 136 ± 14 Ma with initial $^{206}Pb/^{207}Pb$ ratio of 1.602 ± 0.094 (with errors at a 95% confidence level, MSWD = 2.7), which is again much younger than intercept ages (Fig. 3).

In the third group, 30 spots were analyzed using a laser beam diameter of 74 μm, with energy density of 1.8 J/cm^2 and a repetition rate of 12 Hz. Two analyses were excluded because of inclusions ablated during the analyses. The remaining analyses shown relatively low ^{207}Pb counts, due to the low beam energy density. These analyses yielded a U–Pb concordia lower intercept age of 156.4 ± 8.4 Ma (MSWD = 7.9), a U–Pb Tera–Wasserburg concordia lower intercept age of 159.3 ± 8.4 Ma (MSWD = 7.9) and a younger $^{206}Pb/^{207}Pb$–$^{238}U/^{207}Pb$ isochron age of 146 ± 12 Ma with initial $^{206}Pb/^{207}Pb$ ratio of 1.58 ± 0.11 (with errors at a 95% confidence level, MSWD = 2.0) (Fig. 4). The slightly larger errors are attributed to low Pb signals (in particular, ^{207}Pb) because of the low beam energy density.

We also analyzed cassiterite grains of tin skarn from the Hehuaping deposit using a laser beam diameter of 74 μm, with a beam energy density of 4 J/cm^2 and a repetition rate of 6 Hz. Seven spots were excluded based on the criteria mentioned above. The remaining 32 analyses also showed two different trends. Analyses with less common Pb yield a U–Pb concordia lower intercept age of 155 ± 13 Ma (MSWD = 2.6), a U–Pb Tera–Wasserburg concordia lower intercept age of 150.9 ± 8.8 Ma (MSWD = 2.9) and a younger $^{206}Pb/^{207}Pb$–$^{238}U/^{207}Pb$ isochron age of 137 ± 21 Ma with initial $^{206}Pb/^{207}Pb$ of 1.97 ± 0.34 (MSWD = 0.35) (Fig. 5).

A large cassiterite crystal from the Xuebaoding W–Sn–Be deposit was selected for U–Pb dating, using a laser beam diameter of 74 μm, with a beam energy density of 4 J/cm^2 and a repetition rate of 6 Hz. Fifteen of a total of 90 spots were excluded due to extremely low Pb counts. The remaining 75 analyses yielded a U–Pb concordia lower intercept age of 194.8 ± 6.2 Ma (MSWD = 0.39) and a U–Pb Tera–Wasserburg concordia lower intercept age of 194.8 ± 6.4 Ma (MSWD = 0.4) (Fig. 6) (Table 6). This sample has very low common Pb, as a result, no reliable $^{206}Pb/^{207}Pb$–$^{238}U/^{207}Pb$ isochron age has been obtained (Fig. 7).

4. Discussion

4.1. Cassiterite U–Pb dating

In general, high energy densities and faster repetition rates lead to higher signals and smaller errors. Meanwhile, the faster ablation also means more chance to ablate fluid/mineral inclusions and thus introduce non-equilibrium common Pb, which may cause large errors. For cassiterite grains from the Hehuaping greisen, the best results were obtained using beam diameter: 74 μm; energy density: 4 J/cm^2; repetition rate of 6 Hz.

Our $^{206}Pb/^{207}Pb$ versus $^{238}U/^{207}Pb$ "isochron" ages (Figs. 2–5) are systematically younger (~5–10%) than those of concordia and Tera–Wasserburg lower intersection ages. This is likely due to the "isochron" itself. Isochron dating is useful especially for U–Pb systems of minerals with high common Pb contents, like cassiterite (Gulson and Jones, 1992; Yuan et al., 2008). Nevertheless, for in situ analyses using laser ablation systems, both ICP-MC-MS and ICP-(quadrupole)-MS usually have high signals of ^{204}Pb because of ^{204}Hg interference from the Ar gas. Therefore, ^{207}Pb instead of ^{204}Pb was chosen for the isochron (Chen et al., 2014; Yuan et al., 2011; Zhang et al., 2014). Given that $^{206}Pb_i/^{207}Pb$ is not constant, i.e., ^{207}Pb changes with time and U/Pb_i ratios, the larger the U/Pb_i and the older the samples, the smaller the $^{206}Pb_i/^{207}Pb$, resulting in systematically younger "isochron" ages with larger errors introduced by samples with low common Pb. In addition, samples with lower common Pb are the best for U–Pb dating. Using the $^{206}Pb/^{207}Pb$ versus $^{238}U/^{207}Pb$ "isochron", however, the lower the common Pb the larger the statistic errors of $^{206}Pb/^{207}Pb$ and $^{238}U/^{207}Pb$ due to low ^{207}Pb, e.g., no successful U–Pb "isochron" of

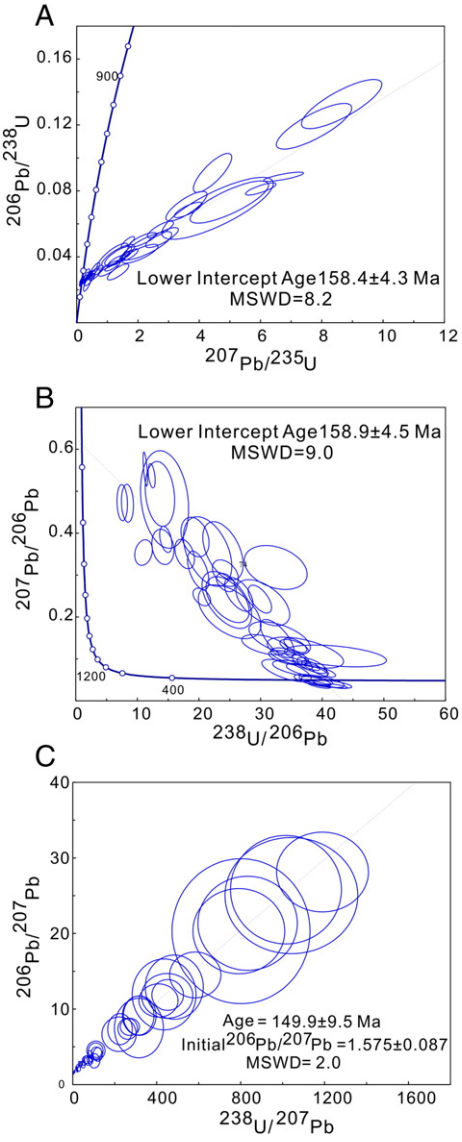

Fig. 2. Concordia, Tera–Wasserburg and $^{206}Pb/^{207}Pb$ versus $^{238}U/^{207}Pb$ "isochron" diagrams for cassiterite from the Hehuaping Sn polymetallic deposit in South China (beam diameter: 74 μm; energy density: 4 J/cm^2; repetition rate of 6 Hz). Intersection ages (A, B) are identical to each other and are ~10 Ma older than that of the $^{206}Pb/^{207}Pb$ versus $^{238}U/^{207}Pb$ "isochron" age (C).

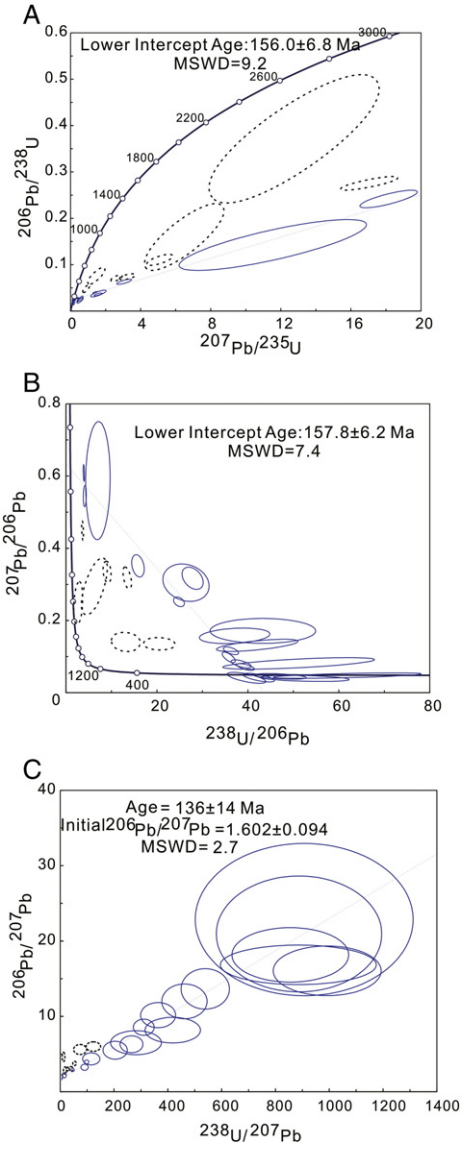

Fig. 3. Concordia, Tera–Wasserburg and $^{206}Pb/^{207}Pb$ versus $^{238}U/^{207}Pb$ "isochron" diagrams for the same cassiterite sample suite as Fig. 2, using similar working conditions except higher energy density (8 J/cm^2). High energy results in higher signal and usually smaller statistic errors. Nevertheless, the results are worse because of high common Pb, likely from tiny inclusions that cannot be identified from the raw data. Thirty analyses can be classified into two groups due to non-equilibrium common Pb. Symbols with solid lines indicated less common Pb. Intersection ages (A, B) are identical to each other and are ~20 Ma older than that of the $^{206}Pb/^{207}Pb$ versus $^{238}U/^{207}Pb$ "isochron" age (C).

cassiterite crystal from Xuebaoding was obtained in this study. Moreover, these larger errors are weighted more heavily in the "isochron". Surprisingly, our new results are consistent with previously published $^{206}Pb/^{207}Pb$ versus $^{238}U/^{207}Pb$ "isochron" age of cassiterite grains from the same sample (154.8 ± 5.8 Ma) within error for Hehuaping (Zhang et al., 2015). Nevertheless, the "isochron" age is ~3 Ma younger. This is likely because of the errors introduced by the "isochron".

In addition, our new LA-ICP-MS concordia and Tera–Wasserburg lower intersection ages are also consistent with recently published $^{206}Pb/^{207}Pb$ versus $^{238}U/^{207}Pb$ "isochron" age of cassiterite for Xuebaoding (193.6 ± 6 Ma, Zhang et al., 2014) samples using LA-MC-ICPMS, within error. The reasons behind this are not clear yet. Nevertheless, LA-MC-ICPMS analyzes Pb isotopes simultaneously, such that it has higher precision. For young cassiterite samples, the effect of ^{207}Pb may be much smaller than the total analytical errors, such that the ages are still reasonable within error. Alternatively, the systematic error and random errors may have gone on opposite directions, resulting in data with small errors.

In principle, ^{208}Pb may serve as common Pb for datings on Th free high U minerals. Nevertheless, Th content of cassiterite is generally at low ppm levels, comparable to that of U. Moreover, the ^{208}Pb signal is unstable for most of our cassiterite samples. The Th concentration in several cassiterite grains is as high as 1 ppm, which is not suitable for ^{208}Pb isochron.

4.2. Tera–Wasserburg diagrams

The Tera–Wasserburg concordia diagram places $^{238}U/^{206}Pb$ and $^{207}Pb/^{206}Pb$ on the x- and y-axes, respectively (Tera and Wasserburg, 1972a,b). The concordia curve is defined by decays of U when there is no common Pb. Therefore, results obtained for closed systems plot on the concordia curve, whereas those obtained from open systems are

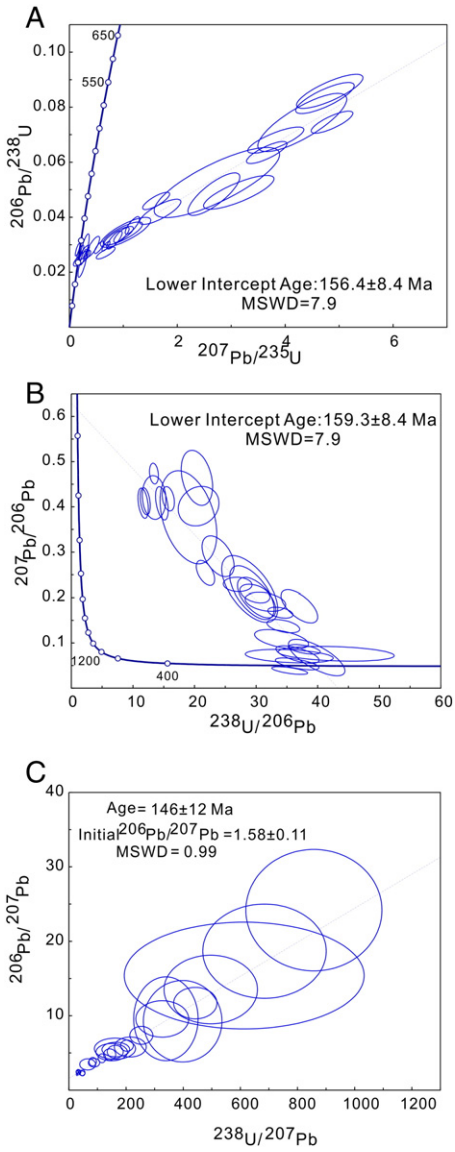

Fig. 4. Concordia, Tera–Wasserburg and $^{206}Pb/^{207}Pb$ versus $^{238}U/^{207}Pb$ isochron diagrams for the same cassiterite sample suite as Fig. 2, using similar working conditions except lower energy density (1.8 J/cm^2). The slightly larger errors are attributed to low Pb signals (in particular, ^{207}Pb), because of the low beam energy density. Again, intersection ages (A, B) are identical to each other and are >10 Ma older than that of the $^{206}Pb/^{207}Pb$ versus $^{238}U/^{207}Pb$ "isochron" age (C).

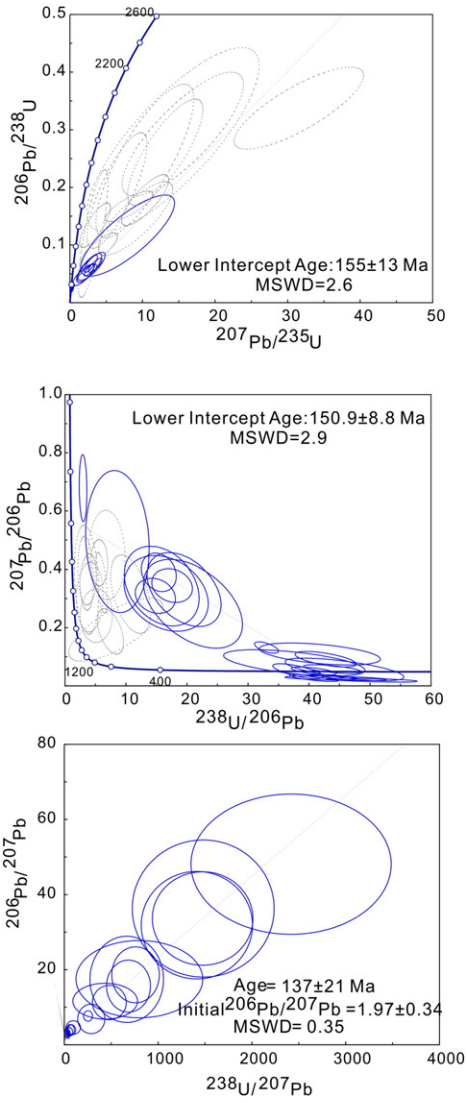

Fig. 5. Concordia, Tera–Wasserburg and $^{206}Pb/^{207}Pb$ versus $^{238}U/^{207}Pb$ isochron diagrams for cassiterite from skarn orebody in Hehuaping (beam diameter: 74 μm; energy density: 4 J/cm^2; repetition rate of 6 Hz). Cassiterite from skarn ore deposit has more than one common Pb sources, magmas, fluids and carbonates. Much larger errors were induced by non-equilibrium common Pb.

discordant, which may define a discordia line whose intersections with the concordia curve indicate the time of formation and that of disturbance of the system. Analyses of a cogenetic suite of samples with different proportions of radiogenic to common Pb define a line that will intercept concordia at the true age and the $^{207}Pb/^{206}Pb$ axis at the composition of Pb_i. The Tera–Wasserburg diagram is very useful for samples with substantial amounts of common Pb, especially for data analyzed using LA-ICP-MS method (Chew et al., 2014), because it requires neither $^{206}Pb/^{204}Pb$, nor a priori common Pb correction.

Given that the Tera–Wasserburg concordia age is the lower intercept age that is controlled by samples with low common Pb, spot analyses with lower common Pb are weighted more heavily. As shown above, Tera–Wasserburg concordia ages are preferred for U–Pb dating of cassiterite and other minerals with high common Pb. Nevertheless, for samples with very high common Pb, Tera–Wasserburg concordia may also produce ages with large errors.

4.3. LA-MC-ICP-MS versus LA-ICP-MS

Multi-collector ICP-MS has an advantage of high precision Pb isotope data, and therefore it is commonly used for minerals with high common Pb contents. Previous studies on in situ cassiterite U–Pb dating so far published have all been carried out using LA-MC-ICP-MS. In addition to cassiterite, other U-bearing accessory phases such as zircon (Machado and Simonetti, 2002), baddeleyite, monazite, titanite (Simonetti et al., 2006), and rutile (Bracciali et al., 2013) have also been dated using LA-MC-ICP-MS method. Nevertheless, MC-ICP-MS also has major ^{204}Pb interference from ^{204}Hg on very low ^{204}Pb signals, such that it cannot provide high quality $^{206}Pb/^{204}Pb$, $^{207}/Pb/^{204}Pb$, $^{238}U/^{204}Pb$ ratios.

As discussed above, the Tera–Wasserburg concordia diagram is the best way to obtain U–Pb ages for minerals with high common Pb. This age is defined by $^{238}U/^{206}Pb$. Therefore, the main errors of U–Pb dating using LA-(MC)-ICP-MS comes from fractionation between Pb and U during laser ablation, which is controlled by different volatilities of these two elements. Given that MC-ICPMS cannot collect U and Pb

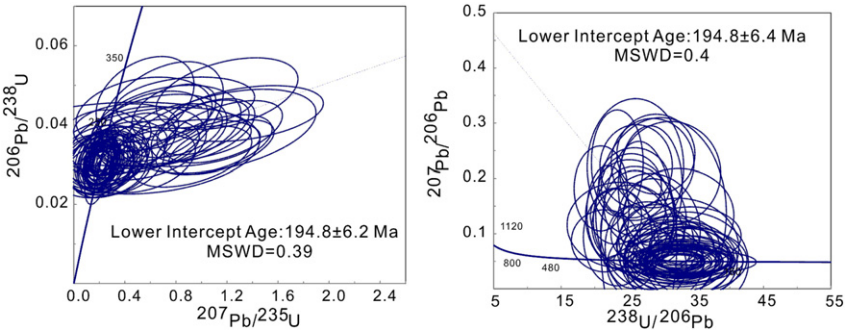

Fig. 6. Concordia and Tera–Wasserburg diagrams for a large cassiterite crystal from the Xuebaoding Sn–W–Be deposit in southwest China (beam diameter: 74 μm; energy density: 4 J/cm^2; repetition rate of 6 Hz). These two diagrams give ages identical to each other.

simultaneously, whereas it takes much longer time for the magnet to switch fields than quadrupole, the $^{238}U/^{206}Pb$ ratios obtained by LA-MC-ICPMS are not necessarily much better than that obtained by LA-ICP-MS. In this case, multi-collector ICP-MS does not have significant advantage over ICP-MS.

LA-ICP-MS is much cheaper than LA-MC-ICP-MS, which has been widely used on U–Pb dating of zircon (Allen and Campbell, 2012; Black et al., 2004; Bryan et al., 2004; Catalan et al., 2004; Liang et al., 2006; Simonetti and Neal, 2010), monazite (Kohn and Vervoort, 2008), perovskite (Cox and Wilton, 2006), baddeleyite (Horn et al., 2000), titanite and rutile (Kooijman et al., 2010; Storey et al., 2007; Zack et al., 2011), loparite (Mitchell et al., 2011) and eudialyte (Wu et al., 2010). Our results in this contribution show that LA-ICP-MS can provide cassiterite U–Pb ages comparable to those obtained using LA-MC-ICP-MS.

4.4. Common lead

For cassiterite and other high common Pb minerals, samples with multiple common Pb sources are difficult to date. Cassiterite from pegmatite, granite and greisen usually has homogenized common Pb. In contrast, those from skarn deposits usually have two sources of common Pb, i.e., granite and carbonate. These non-equilibrium common Pb may introduce large errors (Clayton and Rojkovic, 1999). Our results show that multiple common Pb are often associated with fluid inclusions that may be identified from raw signals and avoided (Fig. 1). In some cases, multiple common Pb cannot be easily identified from the raw data, they may be grouped in the Tera–Wasserburg diagram. Nevertheless, Tera–Wasserburg age is defined by analyses with the least common Pb contents. Therefore, common Pb has less influence on the ages. Nevertheless, for samples with very high common Pb, Tera–Wasserburg concordia diagram may also produce large errors.

4.5. Applications

Cassiterite is an ore mineral, therefore it directly dates the mineralization event. Zircon U–Pb ages usually record magmatic or hydrothermal (for hydrothermal zircon) processes. Fluid inclusion $^{40}Ar/^{39}Ar$ dating results represent hydrothermal events. Therefore, cassiterite dating together with zircon and/or $^{40}Ar/^{39}Ar$ dating results may provide firm constraints on the relation between magmatism, hydrothermal activities and mineralization. Nevertheless, the precisions of cassiterite U–Pb ages range from 2 to 5%, which mainly comes from multiple sources of common Pb. Therefore, it is not very sensitive to mineralization events related to magmatism or magmatic fluids.

The best result for cassiterite from the Hehuaping greisen is 158.9 ± 4.5 Ma. The slightly younger lower intercept ages for tin skarn samples are likely due to non-equilibrium common Pb. Nevertheless, our results are consistent with four zircon U–Pb ages of 155.3 Ma to 157.3 Ma for the parental biotite granite and granite porphyry dykes in the Hehuaping Sn–Pb–Zn deposit, within error.

For the Xuebaoding cassiterite sample, our U–Pb dating results (194.8 ± 6.2 Ma and 194.8 ± 6.4 Ma) are identical to recently published cassiterite LA-MC-ICPMS U–Pb isochron age (193.6 ± 6 Ma) and $^{40}Ar/^{39}Ar$ age of muscovite from the muscovite–cassiterite vein (194.5 ± 1.0 Ma, Zhang et al., 2014). They are slightly older than previously published scheelite Sm–Nd isochron age (182.0 ± 9.2 Ma, Liu et al., 2007a). These U–Pb ages of cassiterite are also similar to previous dating results on granites within error, e.g., Liu et al. (2010) obtained two muscovite $^{40}Ar/^{39}Ar$ plateau ages of 200 Ma and 193 Ma for the parental Pukouling and Pankou muscovite granites in the Xuebaoding Sn–W–Be deposit.

These two samples' cassiterite LA-ICP-MS U–Pb dating results are all similar to previously published ages using other methods, suggesting that these mineralization events were closely associated with magmatic fluids.

5. Conclusions

Cassiterite is the main ore mineral of Sn deposits and can be dated using in situ LA-ICP-MS methods. Tera–Wasserburg U–Pb intercept age is the best way to eliminate common Pb effects. The commonly used $^{206}Pb/^{207}Pb$ versus $^{238}U/^{207}Pb$ "isochron" produces systematically younger ages with larger errors, because $^{206}Pb_i/^{207}Pb$ is not constant. Therefore, the older the samples, and the lower the common Pb, the larger errors the "isochron" produces. Samples with multiple common Pb sources are difficult to date. Nevertheless, multiple common Pb in cassiterite are often associated with fluid inclusions that may be identified and avoided. Common Pb also has much less effects on the Tera–Wasserburg ages. Cassiterite U–Pb ages directly date the mineralization event, which may provide firm constraints on the relation between magmatism ± hydrothermal activity and mineralization, when coupled with other dating methods.

Conflict of interest

There is no conflict of interest.

Acknowledgments

We would like to thank Professor Hui-min Li at Tianjing Institute of Geology and Mineral Resources for his helpful instructions, discussion and cassiterite samples. Thanks also to Dr. Yan Liu at Institute of Geology, Chinese Academy of Geological Sciences for his cassiterite crystal. Professor C.T. Lee and an anonymous referee are thanked for constructive review comments. This study is supported by the National Natural Science Foundation of China (Nos. 41090374, 41421062, 41172080). This is contribution No. IS-2107 from GIGCAS.

Table 6
U–Pb isotopic data of cassiterite from the Xuebaoding W-Sn-Be deposit.

	U (ppm)	Th (ppm)	$^{207}Pb/^{206}Pb$	1σ	$^{207}Pb/^{235}U$	1σ	$^{206}Pb/^{238}U$	1σ
XBD-101*	0.3	0.0	0.00000	0.00000	0.41474	0.64452	0.03772	0.00528
XBD-102	0.4	0.0	2.19353	1.23173	0.67002	0.33132	0.04201	0.00922
XBD-10	0.2	0.0	0.14812	0.13274	0.66469	0.35387	0.03854	0.00606
XBD-104	0.4	0.0	0.22885	0.09993	1.01281	0.23841	0.03936	0.00456
XBD-105*	0.3	0.0	0.00000	0.00000	0.72295	0.38723	0.03971	0.00681
XBD-106	0.4	0.0	0.10210	0.16274	0.60708	0.24821	0.03512	0.00414
XBD-107	0.5	0.0	0.16900	0.18116	0.62398	0.28302	0.03965	0.00587
XBD-108	0.8	0.0	0.73190	0.68448	0.20665	0.17101	0.03146	0.00281
XBD-109	0.3	0.0	0.30460	0.29175	0.63390	0.54422	0.03354	0.00719
XBD-110	0.5	0.0	0.21769	0.11952	0.41528	0.21019	0.03435	0.00431
XBD-111*	0.2	0.0	0.00000	0.00000	1.01182	0.26819	0.03869	0.00523
XBD-112*	0.3	0.0	0.00000	0.00000	0.87322	0.35928	0.04561	0.00428
XBD-113	0.4	0.0	0.23197	0.12475	0.92735	0.30884	0.03207	0.00507
XBD-114*	0.4	0.0	0.00000	0.00000	0.78864	0.24814	0.03855	0.00449
XBD-115*	0.3	0.0	0.00000	0.00000	1.20060	0.36715	0.04790	0.00598
XBD-116*	0.3	0.0	0.00000	0.00000	0.55865	0.25340	0.04655	0.00709
XBD-117	0.3	0.0	0.31504	0.26165	0.25200	0.18670	0.03118	0.00495
XBD-118	0.3	0.0	0.26755	0.08172	1.16639	0.48326	0.03844	0.00697
XBD-119	0.5	0.0	0.31079	0.09719	1.15733	0.27238	0.03442	0.00453
XBD-120	2.5	0.0	0.09566	0.01387	0.41754	0.05421	0.03221	0.00156
XBD-121	0.4	0.0	0.56367	0.55894	0.78441	0.21787	0.04320	0.00469
XBD-122	0.4	0.0	0.20850	0.07722	0.56740	0.25464	0.03086	0.00516
XBD-123	0.4	0.0	0.07290	0.13091	1.09927	0.30061	0.03502	0.00497
XBD-124*	0.2	0.0	0.00000	0.00000	0.50801	0.34997	0.03542	0.00612
XBD-125	0.6	0.0	0.05365	0.09275	0.40866	0.12919	0.03667	0.00361
XBD-126	0.2	0.0	0.53375	0.37464	0.19528	0.25119	0.02975	0.00535
XBD-127	0.4	0.0	0.29815	0.15918	0.49197	0.20211	0.03596	0.00463
XBD-128*	0.5	0.0	0.00000	0.00000	0.21921	0.11688	0.02946	0.00372
XBD-129	0.4	0.0	0.13678	0.05519	0.40950	0.27136	0.03920	0.00404
XBD-130	0.7	0.0	0.14816	0.06447	0.33252	0.10862	0.03043	0.00292
XBD-131	0.6	0.0	0.08101	0.05239	0.37666	0.12901	0.03260	0.00338
XBD-132	0.4	0.0	0.10923	0.07764	0.20508	0.20646	0.03032	0.00495
XBD-133	0.3	0.0	0.89305	0.52278	1.34693	0.40206	0.04286	0.00466
XBD-134	0.3	0.0	0.75175	0.42518	1.17271	0.30516	0.03827	0.00519
XBD-135*	0.5	0.0	0.00000	0.00000	0.91184	0.36321	0.03543	0.00393
XBD-136	0.4	0.0	0.23582	0.10330	0.38746	0.15110	0.02926	0.00424
XBD-137	0.3	0.0	0.12271	0.18876	0.30065	0.11306	0.03306	0.00418
XBD-138*	0.3	0.0	0.00000	0.00000	0.33424	0.16060	0.03119	0.00410
XBD-139	0.3	0.0	0.08036	0.06834	0.31662	0.26015	0.03094	0.00570
XBD-140	0.4	0.0	0.51655	0.50311	0.55090	0.35179	0.04277	0.00614
XBD-141*	0.3	0.0	0.00000	0.00000	0.20937	0.22020	0.03611	0.00506
XBD-142	0.5	0.0	0.04908	0.05453	0.21564	0.13678	0.03096	0.00511
XBD-01	0.2	0.0	0.04939	0.08383	0.20339	0.17526	0.02975	0.00487
XBD-02	0.3	0.0	0.09453	0.03641	0.21106	0.09345	0.03043	0.00490
XBD-03	0.4	0.0	0.08849	0.03551	0.21178	0.08084	0.03067	0.00358
XBD-04	0.4	0.0	0.09975	0.05053	0.21369	0.08258	0.03048	0.00344
XBD-05	0.4	0.0	0.11158	0.04717	0.21260	0.07100	0.03010	0.00392
XBD-06	0.2	0.0	0.83108	0.52566	0.21364	0.11963	0.03086	0.00603
XBD-07	0.3	0.0	0.05354	0.03810	0.20637	0.10402	0.03069	0.00375
XBD-08	0.3	0.0	0.05561	0.01401	0.19603	0.06386	0.03095	0.00312
XBD-11	0.5	0.0	0.08510	0.11351	0.24715	0.22751	0.03242	0.00493
XBD-12	0.4	0.0	0.06257	0.03482	0.25164	0.14998	0.03075	0.00504
XBD-14	0.3	0.0	0.12378	0.05449	0.23196	0.09554	0.03061	0.00378
XBD-15	0.4	0.0	0.09243	0.05978	0.21881	0.07456	0.02943	0.00354
XBD-16	0.3	0.0	0.31355	0.14413	0.20785	0.07663	0.03051	0.00448
XBD-17	0.3	0.0	0.05098	0.01678	0.22345	0.06546	0.03204	0.00319
XBD-18	0.3	0.0	0.10327	0.05286	0.21494	0.06972	0.03070	0.00504
XBD-19	0.7	0.0	0.07176	0.01918	0.20990	0.05109	0.03049	0.00212
XBD-20	0.6	0.0	0.05725	0.01534	0.20721	0.04198	0.03065	0.00232
XBD-22	0.7	0.0	0.05569	0.01431	0.20514	0.05813	0.03028	0.00190
XBD-23	0.9	0.0	0.05091	0.01248	0.20692	0.04230	0.03076	0.00178
XBD-24	0.4	0.0	0.08462	0.03519	0.20738	0.09956	0.03146	0.00407
XBD-25	0.3	0.0	0.05323	0.02333	0.20253	0.08424	0.02979	0.00319
XBD-26	0.3	0.0	0.23809	0.11992	0.21062	0.08836	0.03077	0.00403
XBD-27	0.2	0.0	0.01870	0.00691	0.20026	0.16204	0.02934	0.00353
XBD-28	0.4	0.0	0.05523	0.02162	0.20972	0.08906	0.03087	0.00245
XBD-29	0.4	0.0	0.06884	0.02826	0.20797	0.06084	0.03009	0.00289
XBD-30	0.9	0.0	0.04288	0.00832	0.21251	0.03649	0.03098	0.00233
XBD-31	0.7	0.0	0.07411	0.02375	0.20958	0.04183	0.03047	0.00213
XBD-34	0.3	0.0	0.02745	0.01262	0.22291	0.09236	0.02987	0.00389
XBD-35	0.4	0.0	0.14984	0.06594	0.20645	0.07048	0.03076	0.00306
XBD-36	0.3	0.0	0.02833	0.01008	0.20524	0.08029	0.03065	0.00701
XBD-37	0.3	0.0	0.05461	0.01406	0.20701	0.06978	0.02959	0.00377
XBD-38	0.2	0.0	0.05985	0.01773	0.21644	0.06402	0.03161	0.00272
XBD-40	0.3	0.0	0.06610	0.03262	0.21559	0.16722	0.02996	0.00543

* These data with zero $^{207}Pb/^{206}Pb$ are not used in age calculation. Because the raw data showed that the signal of Pb have a peak at the very beginning, which is caused by the surface contamination by common Pb. When calculating the ratio of $^{207}Pb/^{206}Pb$ by ICPMSDATACAL and the value of $^{207}Pb/^{206}Pb$ cannot be displayed.

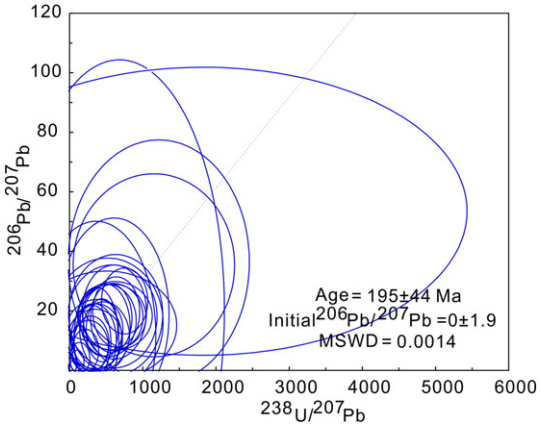

Fig. 7. $^{206}Pb/^{207}Pb$ versus $^{238}U/^{207}Pb$ "isochron" diagrams for the large cassiterite crystal from the Xuebaoding Sn–W–Be deposit in southwest China. Because of the low common Pb, no $^{206}Pb/^{207}Pb$–$^{238}U/^{207}Pb$ "isochron" was obtained.

References

Allen, C.M., Campbell, I.H., 2012. Identification and elimination of a matrix-induced systematic error in LA-ICP-MS $^{206}Pb/^{238}U$ dating of zircon. Chem. Geol. 332, 157–165.

Bai, X.J., Wang, M., Jiang, Y.D., Qiu, H.N., 2013. Direct dating of tin–tungsten mineralization of the Piaotang tungsten deposit, South China, by $^{40}Ar/^{39}Ar$ progressive crushing. Geochim. Cosmochim. Acta 114, 1–12.

Black, L.P., Kamo, S.L., Allen, C.M., Aleinikoff, J.N., Davis, D.W., Korsch, R.J., Foudoulis, C., 2004. Improved $^{206}Pb/^{238}U$ microprobe geochronology by the monitoring of a trace-element-related matrix effect; SHRIMP, ID-TIMS, ELA-ICP-MS and oxygen isotope documentation for a series of zircon standards. Chem. Geol. 205 (1–2), 115–140.

Bracciali, L., Parrish, R.R., Horstwood, M.S.A., Condon, D.J., Najman, Y., 2013. U–Pb LA-(MC)-ICP-MS dating of rutile: new reference materials and applications to sedimentary provenance. Chem. Geol. 347, 82–101.

Bryan, S.E., Allen, C.M., Holcombe, R.J., Fielding, C.R., 2004. U–Pb zircon geochronology of Late Devonian to Early Carboniferous extension-related silicic volcanism in the northern New England Fold Belt. Aust. J. Earth Sci. 51 (5), 645–664.

Catalan, J.R.M., Fernandez-Suarez, J., Jenner, G.A., Belousova, E., Montes, A.D., 2004. Provenance constraints from detrital zircon U–Pb ages in the NW Iberian Massif: implications for Palaeozoic plate configuration and Variscan evolution. J. Geol. Soc. 161, 463–476.

Chen, X.C., Hu, R.Z., Bi, X.W., Li, H.M., Lan, J.B., Zhao, C.H., Zhu, J.J., 2014. Cassiterite LA-MC-ICP-MS U/Pb and muscovite $^{40}Ar/^{39}Ar$ dating of tin deposits in the Tengchong–Lianghe tin district, NW Yunnan, China. Mineral. Deposita 49 (7), 843–860.

Chew, D.M., Petrus, J.A., Kamber, B.S., 2014. U–Pb LA-ICPMS dating using accessory mineral standards with variable common Pb. Chem. Geol. 363, 185–199.

Clayton, R.E., Rojkovic, I., 1999. Experimental Pb isotope studies of cassiterite from Hnilec granite, Slovakia. Mineral Deposits: Processes to Processing vols. 1 and 2 pp. 329–332.

Cox, R.A., Wilton, D.H.C., 2006. U–Pb dating of perovskite by LA-ICP-MS: an example from the Oka carbonatite, Quebec, Canada. Chem. Geol. 235 (1–2), 21–32.

Gulson, B.L., Jones, M.T., 1992. Cassiterite — potential for direct dating of mineral-deposits and a precise age for the Bushveld complex granites. Geology 20 (4), 355–358.

Gulson, B.L., Jones, M.T., 1993. Cassiterite — potential for direct dating of mineral-deposits and a precise age for the Bushveld complex granites — reply. Geology 21 (3), 286-286.

Horn, I., Rudnick, R.L., McDonough, W.F., 2000. Precise elemental and isotope ratio determination by simultaneous solution nebulization and laser ablation-ICP-MS: application to U–Pb geochronology. Chem. Geol. 164 (3–4), 281–301.

Kohn, M.J., Vervoort, J.D., 2008. U-Th-Pb dating of monazite by single-collector ICP-MS: Pitfalls and potential. Geochem. Geophys. Geosys. 9 (4), 1–16.

Kooijman, E., Mezger, K., Berndt, J., 2010. Constraints on the U–Pb systematics of metamorphic rutile from in situ LA-ICP-MS analysis. Earth Planet. Sci. Lett. 293 (3–4), 321–330.

Li, C.Y., Wang, F.Y., Hao, X.L., Ding, X., Zhang, H., Ling, M.X., Zhou, J.B., Li, Y.L., Fan, W.M., Sun, W.D., 2012. The formation of the Dabaoshan porphyry molybdenum deposit induced by slab rollback. Lithos 150, 101–110.

Liang, H.Y., Campbell, I.H., Allen, C., Sun, W.D., Liu, C.Q., Yu, H.X., Xie, Y.W., Zhang, Y.Q., 2006. Zircon Ce^{4+}/Ce^{3+} ratios and ages for Yulong ore-bearing porphyries in eastern Tibet. Mineral. Deposita 41 (2), 152–159.

Liu, Y., Deng, J., Li, C.F., Shi, G.H., Zheng, A.L., 2007a. REE composition in scheelite and scheelite Sm–Nd dating for the Xuebaoding W–Sn–Be deposit in Sichuan. Chin. Sci. Bull. 52 (18), 2543–2550.

Liu, Y.P., Li, Z.X., Li, H.M., Guo, L.G., Xu, W., Ye, L., Li, C.Y., Pi, D.H., 2007b. U–Pb geochronology of cassiterite and zircon from the Dulong Sn–Zn deposit: evidence for Cretaceous large-scale granitic magmatism and mineralization events in southeastern Yunnan province, China. Acta Petrol. Sin. 23 (5), 967–976.

Liu, Y., Deng, J., Zhang, G.B., Shi, G.H., Yang, L.Q., Wang, Q.F., 2010. $^{40}Ar/^{39}Ar$ dating of Xuebaoding granite in the Songpan–Garze Orogenic Belt, Southwest China, and its geological significance. Acta Geograph. Sin. Engl. Ed. 84 (2), 345–357.

Liu, Y., Deng, J., Shi, G.H., Sun, X., Yang, L.Q., 2012a. Genesis of the Xuebaoding W-Sn-Be crystal deposits in Southwest China: Evidence from fluid inclusions, stable isotopes and ore elements. Resour. Geol. 62 (2), 159–173.

Liu, Y., Deng, J., Shi, G.H., Sun, D.S., 2012b. Geochemical and Morphological Characteristics of Coarse-grained Tabular Beryl from the Xuebaoding W–Sn–Be deposit, Sichuan Province, Western China. Int. Geol. Rev. 54 (14), 1673–1684.

Ludwing, K.R., 2003. Isoplot. A Geochronological Toolkit for Microsoft Excel. Special Publication, Berkeley Geochronology Center, pp. 1–70.

Ma, N., Deng, J., Wang, Q.F., Wang, C.M., Zhang, J., Li, G.J., 2013. Geochronology of the Dasongpo tin deposit, Yunnan Province: evidence from zircon LA-ICP-MS U–Pb ages and cassiterite LA-MC-ICP-MS U–Pb age. Acta Petrol. Sin. 29 (4), 1223–1235.

Machado, N., Simonetti, A., 2002. U–Pb dating of zircon by excimer laser ablation MC-ICPMS. Geochim. Cosmochim. Acta 66 (15A), A472-A472.

Mitchell, R.H., Wu, F.Y., Yang, Y.H., 2011. In situ U–Pb, Sr and Nd isotopic analysis of loparite by LA-(MC)-ICP-MS. Chem. Geol. 280 (1–2), 191–199.

Simonetti, A., Neal, C.R., 2010. In-situ chemical, U–Pb dating, and Hf isotope investigation of megacrystic zircons, Malaita (Solomon Islands): evidence for multi-stage alkaline magmatic activity beneath the Ontong Java Plateau. Earth Planet. Sci. Lett. 295 (1–2), 251–261.

Simonetti, A., Heaman, L.M., Chacko, T., Banerjee, N.R., 2006. In situ petrographic thin section U–Pb dating of zircon, monazite, and titanite using laser ablation-MC-ICP-MS. Int. J. Mass Spectrom. 253 (1–2), 87–97.

Storey, C.D., Smith, M.P., Jeffries, T.E., 2007. In situ LA-ICP-MS U–Pb dating of metavolcanics of Norrbotten, Sweden: records of extended geological histories in complex titanite grains. Chem. Geol. 240 (1–2), 163–181.

Tera, F., Wasserburg, G.J., 1972a. U–Th–Pb systematics in 3 Apollo 14 basalts and problem of initial Pb in lunar rocks. Earth Planet. Sci. Lett. 14 (3), 281–304.

Tera, F., Wasserburg, G.J., 1972b. U–Th–Pb systematics in lunar highland samples from Luna-20 and Apollo-16 missions. Earth Planet. Sci. Lett. 17 (1), 36–51.

Tu, X.L., Zhang, H., Deng, W.F., Ling, M.X., Liang, H.Y., Liu, Y., Sun, W.D., 2011. Application of RESOlution in-situ laser ablation ICP-MS in trace element analyses. Geochimica 40 (1), 83–98.

Wang, X.J., Liu, Y.P., Miao, Y.L., Bao, T., Ye, L., Zhang, Q., 2014. In-situ LA-MC-ICP-MS cassiterite U–Pb dating of Dulong Sn–Zn polymetallic deposit and its significance. Acta Petrol. Sin. 30 (3), 867–876.

Wu, F.Y., Yang, Y.H., Marks, M.A.W., Liu, Z.C., Zhou, Q., Ge, W.C., Yang, J.S., Zhao, Z.F., Mitchell, R.H., Markl, G., 2010. In situ U–Pb, Sr, Nd and Hf isotopic analysis of eudialyte by LA-(MC)-ICP-MS. Chem. Geol. 273 (1–2), 8–34.

Xie, L.W., Yin, Q.Z., Yang, J.H., Wu, F.Y., Yang, Y.H., 2013. A tin-mineralized topaz rhyolite dike with coeval topaz granite enclaves at Qiguling in the Qitianling tin district, southern China. Lithos 170, 252–268.

Yao, Y., Chen, J., Lu, J., Wang, R., Zhang, R., 2014. Geology and genesis of the Hehuaping magnesian skarn-type cassiterite–sulfide deposit, Hunan Province, Southern China. Ore Geol. Rev. 58, 163–184.

Yuan, S.D., Peng, J.T., Hao, S., Li, H.M., Geng, J.Z., Zhang, D.L., 2008. A precise U–Pb age on cassiterite from the Xianghualing tin-polymetallic deposit (Hunan, South China). Mineral. Deposita 43 (4), 375–382.

Yuan, S.D., Peng, J.T., Hu, R.Z., Li, H.M., Shen, N.P., Zhang, D.L., 2011. In situ LA-MC-ICP-MS and ID-TIMS U–Pb geochronology of cassiterite in the giant Furong tin deposit, Hunan Province, South China: new constraints on the timing of tin-polymetallic mineralization. Ore Geol. Rev. 43 (1), 235–242.

Zack, T., Stockli, D.F., Luvizotto, G.L., Barth, M.G., Belousova, E., Wolfe, M.R., Hinton, R.W., 2011. In situ U–Pb rutile dating by LA-ICP-MS: ^{208}Pb correction and prospects for geological applications. Contrib. Mineral. Petrol. 162 (3), 515–530.

Zhang, R.Q., Lu, J.J., Wang, R.C., Lu, X.C., Guo, J.C., Li, F.C., Lehmann, B., Yao, Y., Guo, W.M., 2013. Contrasting W and Sn mineralization events and related granitoids in Wangxianling–Hehuaping area, Nanling Range, South China. Mineral Deposit Research for a High-Tech World vols. 1–4 pp. 1343–1346.

Zhang, D.L., Peng, J.T., Coulson, I.M., Hou, L.H., Li, S.J., 2014. Cassiterite U–Pb and muscovite ^{40}Ar–^{39}Ar age constraints on the timing of mineralization in the Xuebaoding Sn–W–Be deposit, western China. Ore Geol. Rev. 62, 315–322.

Zhang, R.Q., Lu, J.J., Wang, R.C., Yang, P., Zhu, J.C., Yao, Y., Gao, J.F., Li, C. Lei, Z.H. Zhang, W.L., 2015. Constraints of in situ zircon and cassiterite U–Pb, molybdenite Re–Os and muscovite ^{40}Ar–^{39}Ar ages on multiple generations of granitic magmatism and related W–Sn mineralization in the Wangxianling area, Nanling Range, South China. Ore Geol. Rev. 65 (Part 4), 1021–1042.